11.D8

African Easterly Waves in the Superparameterized Community Atmosphere Model (SP-CAM)

Rachel R. McCrary* and David A. Randall
Colorado State University, Fort Collins, Colorado

1. Introduction

The West African Monsoon (WAM) is a complicated system involving many interactions between the atmosphere, ocean and land surface on a range of temporal and spatial scales, from individual rain events to global atmospheric dynamics. Coupled general circulation models (CGCMs), which are used to make future climate change projections, have difficulty representing the annual cycle of precipitation over West Africa. Many models place the summertime precipitation maxima over the Gulf of Guinea rather than over the continent (Cook and Vizy, 2006).

One reason why CGCMs have difficulty representing the monsoon is their inability to represent key rain making weather systems, such as African easterly waves (AEWs). AEWs are synoptic scale disturbances with wavelengths of 3000-6000 km, and periods of 3-6 days. They are the dominant mode of atmospheric variability over West Africa during the summer (June - September; JJAS) and are important for organizing precipitation over this region. Current theory suggests that AEWs are initiated by convective heating in central and eastern Africa (Berry and Thorncroft 2005, Hsieh and Cook 2008) and propagate westward feeding off of the barotropic-baroclinic instability associated with the African easterly jet (AEJ; Hall et al. 2006). Previous studies have found that AEWs follow two preferred tracks: one to the north of the AEJ that is associated with baroclinic energy conversions and one to the south that is associated with barotropic energy conversions (Kiladis et al. 2006). While there is a clear connection between AEWs and convection (Mekonnen et al. 2006, Kiladis et al. 2006), our understanding of specific interactions and potential feedbacks for these waves is incomplete (Janicot et al. 2011).

A recent paper by Ruti et al. (2010) found that AEW activity in the CMIP3 models is typically misrepresented in one of two ways: 1) significantly amplified AEW activity over the continent or 2) weak AEW activity to the west of the continent. The authors focused on the kinematic properties of AEWs and not on the specific relationships between AEWs and convection in each model. Given that all of these models parameterize convective processes, it is unlikely that any of them are able to capture the complex multi-scale interactions between AEWs and convection.

We examine how the implementation of the super-parameterization of cloud processes (Grabowski, 2001; Khairoutdinov and Randall, 2001) in the atmospheric component of the Community Climate System Model (CCSM3) improves the representation of the dynamics of the WAM system. The super-parameterized coupled model is called the SP-CCSM (Stan et al. 2010). With a super-parameterization conventional cloud parameterizations are replaced by a simplified cloud resolving model (CRM) in each grid column. Super-parameterization improves the representation of many aspects of the global climate including the MJO (Benedict and Randall, 2009), the Asian Monsoon (DeMott et al. 2011) and the El Nino - Southern Oscillation (Stan et al. 2010). Here we examine the ability of the SP-CCSM to simulate the WAM. We focus on improvements in the representation of summertime precipitation over West Africa, AEW variability, and the structure of AEWs.

2. Models and Observations

We analyze the simulated West African Monsoon and African Easterly Waves in two CGCMs, CCSM version 3, which uses conventional cumulus parameterizations to represent cloud-scale processes and the SP-CCSM. Both models use the semi-Lagrangian dynamical core with a T42 horizontal resolution and 26 levels, coupled to the 3º version of the Parallel Ocean Program (POP) ocean model. We analyze daily mean output from a 26 year simulation with SP-CCSM and a 23 year simulation with CCSM.

Observed dynamical fields are from the European Centre for Medium-Range Weather Forecasts (ECMWF) ERA-Interim reanalysis product (ERA-I; Dee et al., 2011). The NOAA daily mean interpolated OLR data set from 1979-2010 is used as a proxy for convective

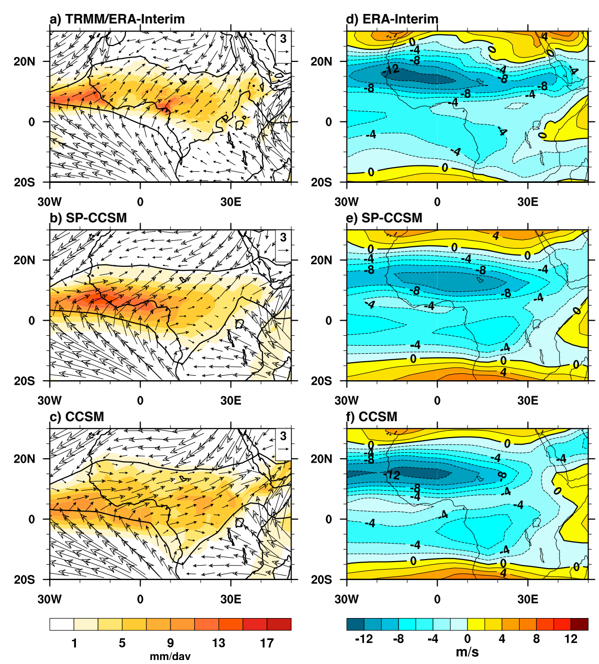

Figure 1. (a-c) JJAS climatological precipitation (filled contours) in mm/day, 925 hPa winds (vectors) and the zero line of zonal wind (line contour) from observations (TRMM and ERA-I), SP-CCSM and CCSM. (d-f) JJAS climatological zonal winds (or AEJ) at 600 hPa in m/s.

* *Corresponding author address*: Rachel R. McCrary, Colorado State University, Dept. of Atmospheric Science, Fort Collins, CO 80523; e-mail: rachel@atmos.colostate.edu

activity (Liebmann, 1996). The precipitation climatology in this study is based on the Tropical Rainfall Measure Mission (TRMM) 3B42 daily mean precipitation data for 1998-2010 between 40ºS-40ºN (Huffman et al., 2007).

3. Results

a. *JJAS Climatology*

The observed seasonal cycle of the WAM has been well documented in previous studies (e.g. Liebmann et al, 2012). Here we briefly examine the structure of summer precipitation, low-level monsoon winds and the AEJ. Figure 1 shows the JJAS climatological precipitation and 925 hPa winds from observations and the models. In the observed monsoon, precipitation moves onto the continent reaching ~20ºN and producing the largest rainfall amounts of the year. Embedded within the observed monsoon are three distinct maxima in precipitation: one over the Ethiopian Highlands, one near the Bight of Bonny near Cameroon, and a third over the Atlantic Ocean. The southwesterly low-level monsoon winds cross the equator, and bring moisture onto the continent. The monsoon winds converge with the dry northerly Harmattan winds just to the north of the 1mm day^{-1} precipitation band.

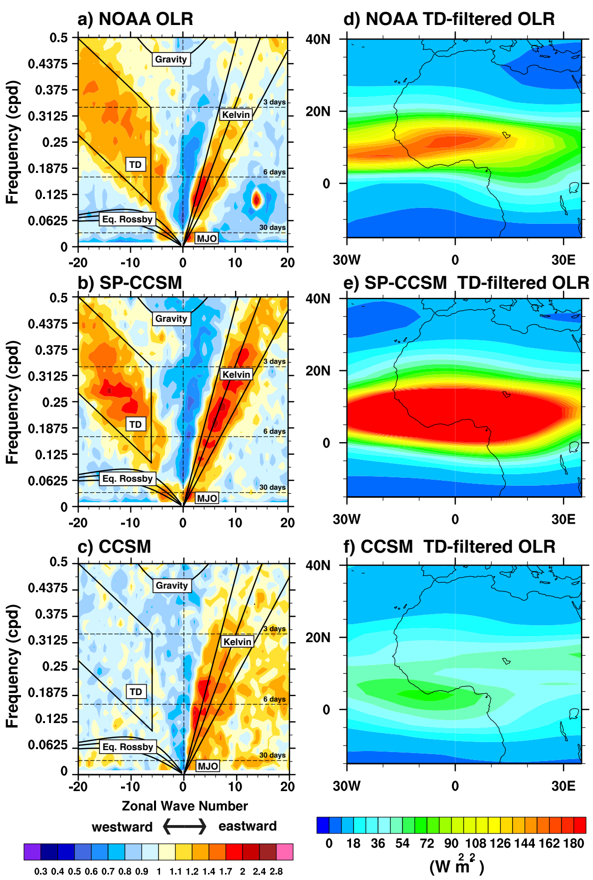

Figure 2. (a-c) JJAS signal-to-noise space-time spectra of OLR averaged between 15ºN-15ºS for waves that are symmetric about the equator from observations(a), SP-CCSM(b) and CCSM(c). To calculate the signal to noise ratio, the JJAS spectra is divided by the smoothed red-noise spectra calculated for the entire year. (d-f) Variance of JJAS TD-filtered OLR in units of (W m^{-2})$^{-2}$

When compared to the standard CCSM, SP-CCSM better represents both the magnitude and the spatial patterns of summer monsoon precipitation over West Africa (Figure 1a-c). The region of maximum precipitation is shifted from the Gulf of Guinea in CCSM (not realistic), to over the continent in SP-CCSM. SP-CCSM captures the local maximum in precipitation over the Atlantic as well as the maximum over the Ethiopian Highlands, although precipitation rates are lower than observed due to the coarse representation of these mountains in the model. SP-CCSM does not simulate the maximum in precipitation near Cameroon nor does it capture the dry region along the Guinea Coast between the two coastal precipitation maxima. AMIP-style simulations done with SP-CAM suggest that these biases are due to a misrepresentation of SSTs in the Gulf of Guinea (a common problem for CGCMs). The low-level monsoon winds and Harmattan winds are reasonably well represented in both models, although wind speeds tend to be faster than observed.

The instabilities associated with the AEJ are not sufficient to trigger AEWs (Hall et al. 2006), but the jet is still believed to be important for the propagation and overall development of AEWs. The jet develops due to the strong temperature and moisture gradients between the ocean and the Sahara desert. In ERA-Interim peak winds reach about 12-14 m s^{-1}(Figure 1d). The winds are positioned at about 15ºN, 600 hPa and spread from the west coast to approximately 5ºE. Easterly winds also extend down to about 850mb, where they give way to the westerly monsoon winds. The AEJ is reasonably well positioned in both CCSM and SP-CCSM. The jet tends to be slightly weaker than observed in SP-CCSM, and extends farther to the east to about 20ºE (Figure 1e).

b. *AEW Variability*

Figure 2(a-c) shows the symmetric JJAS signal-to-noise ratio power spectra from observations and both models for OLR averaged between 15ºN-15ºS. In the observations, significant power is found in the tropical depression or TD range, which includes westward propagating waves with wavelengths of 2000-7000 km and periods of 2-10 days. The TD spectral range has been shown to correspond well with AEW activity (Kiladis et al. 2006). The standard CCSM exhibits little-to-no power in the MJO, the ER wave or inertio-gravity waves. It does have significant power in the Kelvin wave region, although at shorter wavelengths than observed. There is no coherent easterly wave power in the CCSM. In the SP-CCSM tropical wave variability is more realistic. In particular, TD activity is present in the SP-CCSM suggesting that AEW activity should be present in this model.

Figure 2(d-f) shows the variance of TD filtered OLR over Africa. In the observations, during JJAS, there is a clear signal of easterly wave activity over West Africa that extends into the Atlantic Ocean. Over West Africa, TD-filtered OLR captures approximately 20-30% of the total variance. The SP-CCSM strongly overestimates the variability of easterly wave activity over West Africa and the East Atlantic (Figure 2e). The variance in TD-filtered OLR is more than 4 times what is observed. Also, TD-filtered variance in OLR captures more than 50% of the total variance in OLR over West Africa. This indicates that too much of the variability in convection over West Africa in SP-CCSM is due to AEW activity. There is also a southward shift in TD filtered OLR over Africa which corresponds with the region of the precipitation maximum in SP-CCSM. Easterly wave activity in CCSM is weak compared to observations. Over Africa, the only signal in the TD filtered OLR occurs over the Gulf of Guinea where precipitation is a maximum. This variance is less than half of what is observed. We have obtained similar results using traditional kinematic indices of AEW activity, such as the variance in 2-6 day bandpass filtered 700hPa meridional wind.

c. Structure of AEWs

Unfiltered OLR anomalies, winds and streamfunction were regressed onto the TD-filtered OLR time series from the basepoint 10ºN,10ºW. The standard deviation of the TD-filtered OLR anomaly time series from the basepoint of the observations and each model was used to scale the results. This allows us to compare the typical “scale” of the waves between the observations and the models (Kiladis et al. 2006, Serra et al. 2010). The point 10ºN, 10ºW was used in the Kiladis et al. (2006) study. It is in a region of high OLR variability and is south of the AEJ where barotropic energy conversions occur.

Figure 3 shows the horizontal structure of AEWs. The 850hPa streamfunction and winds were regressed onto the basepoint time series at zero lag. In the observations, there is a large area of negative OLR anomalies centered over the basepoint, indicating enhanced convection. East and west of the convective signal are regions of suppressed convection. The convective signal is co-located with an anomalous cyclone, which indicates that convection occurs within the trough of the wave. The suppressed convection to the east of the convective signal is associated with an anomalous anti-cyclone. If we follow the development of this wave at various lags (not shown) we see that the region of enhanced convection first appears 3-4 days earlier in central/eastern Africa and propagates along this latitude band. Convection shifts from ahead of the trough over central Africa, to centered within the trough near the west coast of Africa, and then to the rear of the trough over the Atlantic. The position of peak convection relative to the trough axis is supported by vertical cross sections along 10ºN of meridional wind (Figure 4a), regressed onto the TD-filtered OLR time series.

The vertical structure of observed AEWs south of the AEJ exhibit the distinctive first baroclinic mode, with meridional winds changing with height. At low levels, there is little tilt in the meridional winds, indicating that barotropic energy conversions are important for AEWs in this region (Figure 4a). North of the AEJ, baroclinic energy conversions appear to be more important for AEW development and propagation (not shown).

Remember that we scaled the regression analyses in this study by the unique standard deviations at each base basepoint. At 10ºN, 10ºW the variability in the TD-filtered OLR time series for SP-CCSM is approximately twice what is observed, whereas in CCSM the variability is only half of what is observed. We have scaled the corresponding figures (Figure 4 b, c) by these factors,

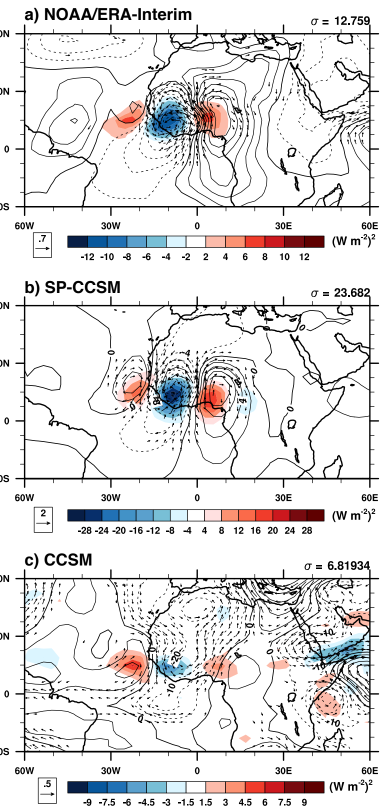

Figure 3. Anomalous OLR, 850 hPa winds and streamfunction regressed onto the TD-filtered OLR time series at the basepoint 10ºN and 10ºW for observations(a), SP-CCSM(b) and CCSM(c). Scales for each figure are based on the standard deviation of the basepoint TD-filtered time series and are different for observations and each model. Stream function contours are by .5x10^{4}m^{2}s^{-1} for Observations and CCSM, and 2x10^{5}m^{2}s^{-1} for SPCCSM.

because it allows us to focus on the differences in the pattern correlations rather than the differences in the magnitudes.

Despite large differences in the magnitudes, Fig. 3b shows that the horizontal structures of the simulated waves that pass over 10ºN, in SP-CCSM, are realistic. As observed, there is a region of enhanced convection centered near the west coast, and flanked on each side by regions of subsidence. The region of enhanced convection is co-located with a perturbation cyclone, and each region of suppressed convection is co-located with an anomalous anti-cyclone. Compared to observations, the OLR anomalies in SP-CCSM are shifted somewhat to the south of the center of each circulation pattern. Tracing back the development of these waves, this pattern develops 3-4 days earlier over central/eastern Africa, and propagates westward. Over land convection is typically within the trough axis and over the Atlantic convection shift to behind the trough. As observed, along 10ºN vertical cross sections of the meridional wind display the first baroclinic mode (Figure 4b). There is very little tilt to the winds at low levels, indicating that barotropic mechanisms are important (not shown).

In CCSM (Figure 3c), there is a weak convective signal that is similar to the observations,but the

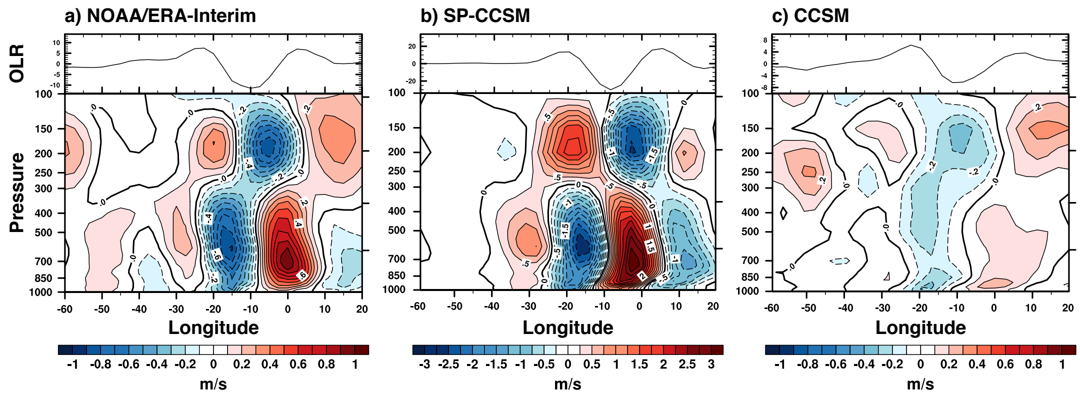

Figure 4. Cross sections of meridional wind along 10ºN regressed on to the TD filtered time series at lag zero. Units are m/s. Time series of OLR anomalies along 10ºN regressed onto the TD filtered time series, units of Wm^{-2}. Each figure is scaled by the basepoint time series.

associated circulation is different, and less coherent than observed. The results from the regression analysis are also noisier than in the observations, and there are peculiar anomalies over the Indian ocean and the Horn of Africa. Tracing back the development of this pattern, we find that there is no real clear corresponding pattern at lags longer than 1 day. Vertical cross sections of the meridional wind suggest that the circulations are barotropic (Figure 4c).

4. Summary and future work

We have shown that the implementation of a super-parameterization in the CCSM results in a number of improvements in the simulation of the WAM and AEWs. In SP-CCSM, the precipitation maximum has a more realistic location, and AEWs are produced. Although AEWs in SP-CCSM are too strong, their horizontal and vertical structures are comparable to observations.

The next steps for this research are to expand the analysis to different basepoints over West Africa, in particular to regions north of the AEJ, to perform energy budget calculations to determine the specific impacts of barotropic and baroclinic energy conversions for the waves in SP-CCSM, and to investigate the characteristics of the convective activity associated with different stages of wave development. We are also planning to make more use of TRMM data.

Acknolwedgements:

The authors would like to thank NOAA, ECMWF, and TRMM for providing the data in this study and Cristiana Stan for providing the model output. We express our gratitude to the NSF science and technology center CMMAP for supporting this research.

5. References

Benedict, J. J., and D. A. Randall, 2009: Structure of the Madden–Julian oscillation in the superparameterized CAM. *J. Atmos. Sci.*, **66**, 3277–3296.

Berry, G. B. and C. Thorncroft, 2005: Case Study of an Intense African Easterly Wave. *Mon. Weath. Rev.,* **133**, 752-766

Cook, K. H. and E. K. Vizy, 2006: Coupled model simulations of the West African monsoon system: Twentieth- and twenty-first-century simulations. J. Climate, **19**, 3681-3703.

Dee, D. P. and coauthors, 2011: The ERA-Interim reanalysis: configuration and performance of the data assimilation system. *Quart. J. Royal. Met. Soc.*, **137**, 553-597.

DeMott, C. A., C. Stan, D. A. Randall, J. L. Kinter, M. Khairoutdinov, 2011: The Asian Monsoon in the Superparameterized CCSM and Its Relationship to Tropical Wave Activity. *J. Climate*, **24**, 5134–5156.

Grabowski, W. W., 2001: Coupling cloud processes with the large-scale dynamics using the cloud-resolving convection parameterization (CRCP). *J. Atmos. Sci.*, **58**, 978–997.

Hall, N. M. J., G. N. Kiladis, C. D. Thorncroft, 2006: Three-Dimensional Structure and Dynamics of African Easterly Waves. Part II: Dynamical Modes. *J. Atmos. Sci.*, **63**, 2231–2245.

Hsieh, Jen-Shan, Kerry H. Cook, 2008: On the Instability of the African Easterly Jet and the Generation of African Waves: Reversals of the Potential Vorticity Gradient. *J. Atmos. Sci.*, **65**, 2130–2151.

Huffman, G.J., R.F. Adler, D.T. Bolvin, G. Gu, E.J. Nelkin, K.P. Bowman, Y. Hong, E.F. Stocker, D.B. Wolff, 2007: The TRMM Multi-satellite Precipitation Analysis: Quasi- Global, Multi-Year, Combined-Sensor Precipitation Estimates at Fine Scale. *J. Hydrometeor.*, **8**: 38-55.

Janicot, S. J. Lafore, C. Thorncroft, 2011: The West African Monsoon. *"The Global Monsoon System: Research and Forecasts, 2nd Edition"*. World Scientific Publishing. Ch 25.

Khairoutdinov, M.F. and D. A. Randall, 2001: A cloud resolving model as a cloud parameterization in the NCAR Community Climate System Model: Preliminary Results. *Geophys. Res. Lett.*, **28**, 3617-3620.

Kiladis, George N., Chris D. Thorncroft, Nicholas M. J. Hall, 2006: Three-Dimensional Structure and Dynamics of African Easterly Waves. Part I: Observations. *J. Atmos. Sci.*, **63**, 2212–2230.

Liebmann B. and C.A. Smith, 1996: Description of a Complete (Interpolated) Outgoing Longwave Radiation Dataset. *BAMS,* **77**, 1275-1277.

Liebmann, B., I. Bladé, G. N. Kiladis, L. M. V. Carvalho, G. Senay, D. Allured, and S. Leroux, 2012: Climatology of African precipitation. *J. Climate*, (in press)

Mekonnen, Ademe, Chris D. Thorncroft, Anantha R. Aiyyer, 2006: Analysis of Convection and Its Association with African Easterly Waves. *J. Climate*, **19**, 5405–5421.

Ruti, Paolo M., Alessandro Dell'Aquila, 2010: The twentieth century African easterly waves in reanalysis systems and IPCC simulations, from intra-seasonal to inter-annual variability. *Clim Dyn.*, **35**, 1099-1117

Stan, C., M. Khairoutdinov, C. A. DeMott, V. Krishnamurthy, D. M. Straus, D. A. Randall, J. L. Kinter III, and J. Shukla, 2010: An ocean-atmosphere climate simulation with an embedded cloud resolving model. *Geophys. Res. Lett.*, **37**, L01702, doi:10.1029/2009GL040822.